EPJ manuscript No.
(will be inserted by the editor)

The Q^2–dependence of the generalised Gerasimov–Drell–Hearn integral for the deuteron, proton and neutron

Draft Version 1.8

The HERMES Collaboration

A. Airapetian,[32] N. Akopov,[32] Z. Akopov,[32] M. Amarian,[26,32] V.V. Ammosov,[24] E.C. Aschenauer,[6] R. Avakian,[32] A. Avetissian,[32] E. Avetissian,[32] P. Bailey,[15] V. Baturin,[23] C. Baumgarten,[21] M. Beckmann,[5] S. Belostotski,[23] S. Bernreuther,[29] N. Bianchi,[10] H. Blok,[22,30] H. Böttcher,[6] A. Borissov,[19] O. Bouhali,[22] M. Bouwhuis,[15] J. Brack,[4] S. Brauksiepe,[11] A. Brüll,[18] I. Brunn,[8] G.P. Capitani,[10] H.C. Chiang,[15] G. Ciullo,[9] G.R. Court,[16] P.F. Dalpiaz,[9] R. De Leo,[3] L. De Nardo,[1] E. De Sanctis,[10] E. Devitsin,[20] P. Di Nezza,[10] M. Düren,[13] M. Ehrenfried,[6] A. Elalaoui-Moulay,[2] G. Elbakian,[32] F. Ellinghaus,[6] U. Elschenbroich,[11] J. Ely,[4] R. Fabbri,[9] A. Fantoni,[10] A. Fechtchenko,[7] L. Felawka,[28] H. Fischer,[11] B. Fox,[4] J. Franz,[11] S. Frullani,[26] Y. Gärber,[8] G. Gapienko,[24] V. Gapienko,[24] F. Garibaldi,[26] E. Garutti,[22] G. Gavrilov,[23] V. Gharibyan,[32] G. Graw,[21] O. Grebeniouk,[23] P.W. Green,[1,28] L.G. Greeniaus,[1,28] A. Gute,[8] W. Haeberli,[17] K. Hafidi,[2] M. Hartig,[28] D. Hasch,[10] D. Heesbeen,[22] F.H. Heinsius,[11] M. Henoch,[8] R. Hertenberger,[21] W.H.A. Hesselink,[22,30] A. Hillenbrand,[8] Y. Holler,[5] B. Hommez,[12] G. Iarygin,[7] A. Izotov,[23] H.E. Jackson,[2] A. Jgoun,[23] R. Kaiser,[14] E. Kinney,[4] A. Kisselev,[23] P. Kitching,[1] K. Königsmann,[11] H. Kolster,[18] M. Kopytin,[23] V. Korotkov,[6] E. Kotik,[1] V. Kozlov,[20] B. Krauss,[8] V.G. Krivokhijine,[7] L. Lagamba,[3] L. Lapikas,[22] A. Laziev,[22,30] P. Lenisa,[9] P. Liebing,[6] T. Lindemann,[5] W. Lorenzon,[19] N.C.R. Makins,[15] H. Marukyan,[32] F. Masoli,[9] F. Menden,[11] V. Mexner,[22] N. Meyners,[5] O. Mikloukho,[23] C.A. Miller,[1,28] Y. Miyachi,[29] V. Muccifora,[10] A. Nagaitsev,[7] E. Nappi,[3] Y. Naryshkin,[23] A. Nass,[8] K. Negodaeva,[6] W.-D. Nowak,[6] K. Oganessyan,[5,10] H. Ohsuga,[29] G. Orlandi,[26] S. Podiatchev,[8] S. Potashov,[20] D.H. Potterveld,[2] M. Raithel,[8] D. Reggiani,[9] P. Reimer,[2] A. Reischl,[22] A.R. Reolon,[10] K. Rith,[8] G. Rosner,[14] A. Rostomyan,[32] D. Ryckbosch,[12] I. Sanjiev,[2,23] F. Sato,[29] I. Savin,[7] C. Scarlett,[19] A. Schäfer,[25] C. Schill,[11] G. Schnell,[6] K.P. Schüler,[5] A. Schwind,[6] J. Seibert,[11] B. Seitz,[1] R. Shanidze,[8] T.-A. Shibata,[29] V. Shutov,[7] M.C. Simani,[22,30] K. Sinram,[5] M. Stancari,[9] M. Statera,[9] E. Steffens,[8] J.J.M. Steijger,[22] J. Stewart,[6] U. Stösslein,[4] K. Suetsugu,[29] H. Tanaka,[29] S. Taroian,[32] A. Terkulov,[20] S. Tessarin,[9] E. Thomas,[10] A. Tkabladze,[6] M. Tytgat,[12] G.M. Urciuoli,[26] P. van der Nat,[22,30] G. van der Steenhoven,[22] R. van de Vyver,[12] M.C. Vetterli,[27,28] V. Vikhrov,[23] M.G. Vincter,[1] J. Visser,[22] M. Vogt,[8] J. Volmer,[6] C. Weiskopf,[8] J. Wendland,[27,28] J. Wilbert,[8] T. Wise,[17] S. Yen,[28] S. Yoneyama,[29] B. Zihlmann,[22,30] H. Zohrabian,[32] P. Zupranski[31]

[1]Department of Physics, University of Alberta, Edmonton, Alberta T6G 2J1, Canada
[2]Physics Division, Argonne National Laboratory, Argonne, Illinois 60439-4843, USA
[3]Istituto Nazionale di Fisica Nucleare, Sezione di Bari, 70124 Bari, Italy
[4]Nuclear Physics Laboratory, University of Colorado, Boulder, Colorado 80309-0446, USA
[5]DESY, Deutsches Elektronen-Synchrotron, 22603 Hamburg, Germany
[6]DESY Zeuthen, 15738 Zeuthen, Germany
[7]Joint Institute for Nuclear Research, 141980 Dubna, Russia
[8]Physikalisches Institut, Universität Erlangen-Nürnberg, 91058 Erlangen, Germany
[9]Istituto Nazionale di Fisica Nucleare, Sezione di Ferrara and Dipartimento di Fisica, Università di Ferrara, 44100 Ferrara, Italy
[10]Istituto Nazionale di Fisica Nucleare, Laboratori Nazionali di Frascati, 00044 Frascati, Italy
[11]Fakultät für Physik, Universität Freiburg, 79104 Freiburg, Germany
[12]Department of Subatomic and Radiation Physics, University of Gent, 9000 Gent, Belgium
[13]Physikalisches Institut, Universität Gießen, 35392 Gießen, Germany
[14]Department of Physics and Astronomy, University of Glasgow, Glasgow G128 QQ, United Kingdom
[15]Department of Physics, University of Illinois, Urbana, Illinois 61801, USA
[16]Physics Department, University of Liverpool, Liverpool L69 7ZE, United Kingdom
[17]Department of Physics, University of Wisconsin-Madison, Madison, Wisconsin 53706, USA
[18]Laboratory for Nuclear Science, Massachusetts Institute of Technology, Cambridge, Massachusetts 02139, USA
[19]Randall Laboratory of Physics, University of Michigan, Ann Arbor, Michigan 48109-1120, USA
[20]Lebedev Physical Institute, 117924 Moscow, Russia
[21]Sektion Physik, Universität München, 85748 Garching, Germany
[22]Nationaal Instituut voor Kernfysica en Hoge-Energiefysica (NIKHEF), 1009 DB Amsterdam, The Netherlands
[23]Petersburg Nuclear Physics Institute, St. Petersburg, Gatchina, 188350 Russia

[24]Institute for High Energy Physics, Protvino, Moscow oblast, 142284 Russia
[25]Institut für Theoretische Physik, Universität Regensburg, 93040 Regensburg, Germany
[26]Istituto Nazionale di Fisica Nucleare, Sezione Roma 1, Gruppo Sanità and Physics Laboratory, Istituto Superiore di Sanità, 00161 Roma, Italy
[27]Department of Physics, Simon Fraser University, Burnaby, British Columbia V5A 1S6, Canada
[28]TRIUMF, Vancouver, British Columbia V6T 2A3, Canada
[29]Department of Physics, Tokyo Institute of Technology, Tokyo 152, Japan
[30]Department of Physics and Astronomy, Vrije Universiteit, 1081 HV Amsterdam, The Netherlands
[31]Andrzej Soltan Institute for Nuclear Studies, 00-689 Warsaw, Poland
[32]Yerevan Physics Institute, 375036 Yerevan, Armenia

Received: June 20, 2002/ Revised version:

Abstract. The Gerasimov–Drell–Hearn (GDH) sum rule connects the anomalous magnetic moment κ of the nucleon with an energy–weighted integral of the difference of the helicity–dependent photoabsorption cross sections. Originally derived for real photons, the GDH integral can be generalised to the case of virtual photons. It then is related to the first moment Γ_1 of the spin structure function $g_1(x,Q^2)$ in deep inelastic scattering (DIS). The first data set taken at HERMES for the deuteron combined with previous measurements on the proton, taken over a large range in photon virtuality Q^2 and photon energy ν is presented providing an unprecedented measurement of the generalised GDH integral for $1.2 < Q^2 < 12.0$ GeV^2 and for photon–nucleon centre–of–mass energies W ranging from $1 < W^2 < 45$ GeV^2 thus covering the resonance as well as the deep inelastic scattering regions. These data allow the study of the Q^2–dependence of the full GDH integral, which is sensitive to both the Q^2–evolution of the resonance form factors and contributions of higher twist. The resonance region contribution is seen to decrease rapidly with increasing Q^2 whereas the DIS contribution remains sizeable down to the lowest measured Q^2. At higher Q^2 the data are found to be in agreement with measurements of the first moment of g_1. From data on the deuteron and proton, the GDH integral for the neutron has been derived and the proton–neutron difference evaluated. This difference is related to the fundamental Bjorken sum rule at high Q^2.

1 Introduction

The Gerasimov–Drell–Hearn (GDH) sum rule connects an energy–weighted integral of the difference of the helicity–dependent real–photon absorption cross sections with the anomalous contribution to the magnetic moment κ of the nucleon :

$$\int_{\nu_0}^{\infty} [\sigma_{\frac{1}{2}}(\nu) - \sigma_{\frac{3}{2}}(\nu)] \frac{d\nu}{\nu} = -\frac{2\pi^2\alpha}{M^2}\kappa^2, \qquad (1)$$

where $\sigma_{\frac{1}{2}(\frac{3}{2})}$ is the photoabsorption cross section for total helicity of the photon-nucleon system equal to $\frac{1}{2}$ ($\frac{3}{2}$), ν is the photon energy, M is the nucleon mass, α the electromagnetic fine–structure constant and ν_0 is the threshold for the lowest lying inelastic channel [1].

The GDH sum rule holds without assumption on the type of target, i.e. it is valid for protons, neutrons or nuclei. For target spins other than $\frac{1}{2}$ the helicity states have to be calculated from parallel ($\sigma_{\uparrow\uparrow}$) and anti–parallel ($\sigma_{\uparrow\downarrow}$) spin configurations of beam and target, respectively. The GDH sum rule is derived from the Compton forward–scattering amplitude following the general physics principles of Lorentz and gauge invariance and is non–perturbative in nature. For the proton ($\kappa_p = +1.79$) the GDH sum rule prediction is $-204\,\mu$b, for the neutron($\kappa_n = -1.91$) it is $-233\,\mu$b. The prediction for the deuteron ($\kappa_d = -0.143$) is $-0.65\,\mu$b. It should be noted that for nuclear targets the lowest–lying inelastic channel is the break–up reaction, in contrast to photoabsorption on the nucleon where the lowest–lying inelastic channel corresponds to single pion production.

No test of the GDH sum rule was hitherto performed due to the lack of polarised targets and suitable real–photon beams. Only recently, first results of an experiment on polarised protons in a limited beam energy range have been published [2]. Using extrapolations into the unmeasured regions, Eq. (1) for the proton seems to be satisfied within the experimental uncertainties. Further real–photon experiments are underway at various laboratories to extend the energy range of the measurements [3,4].

The generalisation of the GDH integral to non–zero photon virtuality Q^2 allows to connect the static ground state properties of the nucleon with its helicity structure as measured in inelastic scattering in the resonance and deep inelastic regions. It then reads [5,6]:

$$I_{GDH}(Q^2) = \int_{\nu_0}^{\infty} [\sigma_{\uparrow\downarrow}(\nu, Q^2) - \sigma_{\uparrow\uparrow}(\nu, Q^2)] \frac{d\nu}{\nu} = \frac{8\pi^2\alpha}{M} \int_0^{x_0} \frac{g_1(x, Q^2) - \gamma^2 g_2(x, Q^2)}{K} \frac{dx}{x}, \qquad (2)$$

where g_1 and g_2 are the polarised structure functions of the nucleon, $\gamma^2 = Q^2/\nu^2$, $x = Q^2/2M\nu$, $x_0 = Q^2/2M\nu_0$ and K is the virtual–photon flux factor.

Examining the generalised GDH integral provides a way to study the transition from polarised real–photon absorption ($Q^2 = 0$) on the nucleon to polarised deep in-

elastic lepton scattering (DIS). In other words, it constitutes an observable that allows the study of the transition from the non–perturbative regime at low Q^2 to the perturbative regime at high Q^2 . Since the generalised GDH integral for the deuteron (proton) is calculated from photoabsorption cross sections, quasielastic (elastic) scattering is excluded from its calculation. As has been pointed out in Ref. [7], the elastic contribution becomes the dominant one below $Q^2 \simeq 0.5$ GeV^2 and has to be taken into account when comparing with twist expansions of the first moment of the spin structure function g_1. In the kinematic region considered in this paper, elastic contributions are expected to be small.

In the leading–twist approximation, the Burkhardt – Cottingham sum rule

$$\int_0^1 g_2(x,Q^2)dx = 0 \tag{3}$$

holds and Eq. (2) simplifies to

$$I_{GDH}(Q^2)_{\gamma^2\to 0} = \frac{16\pi^2\alpha}{Q^2}\Gamma_1. \tag{4}$$

The first moment of the the spin structure function g_1, $\Gamma_1 = \int_0^1 g_1(x)dx$, is predicted to have only a logarithmic Q^2 dependence from QCD evolution. Since for the proton (p) $\Gamma_1^p > 0$ for higher Q^2, I^p_{GDH} must change sign as Q^2 approaches zero in order to reach the negative value predicted by the GDH sum rule at the real–photon point. For the neutron (n) Γ_1^n is negative for all measured Q^2.

The difference of the GDH sum rule for the proton and the neutron, $I^p_{GDH} - I^n_{GDH}$, is of great interest. In the real–photon case, the sum rule gives $I^p_{GDH} - I^n_{GDH} = 29\mu$b, with a sign opposite to what results from multipole analysis of meson photoproduction data [8]. In the Bjorken limit the difference $\Gamma_1^p - \Gamma_1^n$ is given by the Bjorken sum rule. It can be derived using only current algebra and isospin symmetry and consequently constitutes a firm prediction of QCD [9]. This sum rule relates the difference of the first moments of g_1^p and g_1^n at fixed Q^2 to the well–measured neutron beta–decay coupling constant $g_a = |g_A/g_V| = 1.2670 \pm 0.0035$ [10]:

$$\Gamma_1^p - \Gamma_1^n = \frac{1}{6}\cdot g_a \cdot C_{ns}(\alpha_s(Q^2)), \tag{5}$$

where C_{ns} is the non–singlet QCD correction calculated up to $\mathcal{O}(\alpha_s^3)$ in the modified minimal subtraction ($\overline{MS}$) scheme [11]. Experimental verification provides a fundamental test of QCD. Recent measurements confirm the sum rule when perturbative QCD corrections are included [12–14].

Various generalisations of the GDH integral (Eq. (2)) have been considered in the literature. The difference lies in the choice made for the virtual–photon flux factor K. I_A corresponds to the case $K = \nu$. The Gilman notation $K = \nu\sqrt{1+\gamma^2}$ [15] has been used for I_B while for I_C the Hand convention $K = \nu(1-x)$ [16] was chosen. In the notation of Ref. [6] these generalisations read:

$$I_A(Q^2) = \frac{2M^2}{Q^2}\int_0^{x_0}(g_1 - \gamma^2 g_2)dx, \tag{6}$$

$$I_B(Q^2) = \frac{2M^2}{Q^2}\int_0^{x_0}\frac{1}{\sqrt{1+\gamma^2}}(g_1 - \gamma^2 g_2)dx, \tag{7}$$

$$I_C(Q^2) = \frac{2M^2}{Q^2}\int_0^{x_0}\frac{1}{1-x}(g_1 - \gamma^2 g_2)dx. \tag{8}$$

They all agree in the limits of deep inelastic scattering and real–photon absorption, but lead to different numerical results for intermediate Q^2. For the proton, in particular, they lead to different values for the expected zero crossing needed to connect the negative value predicted by Eq. (1) with the positive value required by measurements of Γ_1^p in the DIS limit. The generalisation used throughout this paper is I_B, which is most closely related to photoabsorption cross sections. The full numerical results will be given for all three prescriptions.

The Q^2–dependence of the generalized GDH integral can be studied separately in the DIS region, characterised by large photon–nucleon centre-of-mass energy $W^2 = M^2 + 2M\nu - Q^2$, and in the resonance region where W^2 amounts to only a few GeV^2. Several experiments in progress to measure the generalised GDH integral at low and intermediate Q^2, cover kinematically only the low–W^2 region [17, 18]. On the other hand, the high–W^2 contribution to the generalised GDH integral is found to be sizeable and essential to any estimate of the total integral [19,20]. Preliminary data from real–photon experiments at higher energies support this statement [3]. The kinematics of the HERMES experiment allow to study the Q^2–developement of the generalized GDH integral simultaneously in both, the resonance and DIS region.

2 Experiment

HERMES data on the deuteron target were taken in 1998 to 2000 with a 27.57 GeV beam of longitudinally polarised positrons incident on a longitudinally polarised atomic Deuterium gas target internal to the HERA storage ring at DESY. Data on the proton were taken in 1997 using a longitudinally polarised atomic Hydrogen target. The lepton beam polarisation was measured continously using Compton backscattering of circularly polarised laser light [21,22]. The average beam polarisation for the deuteron (proton) data set was 0.55 (0.55) with a systematic uncertainty of 2.0% (3.4%).

The HERMES polarised gas target [23] consists of polarised atomic D or H confined in a storage cell. It is fed with nuclear–polarised atoms by an atomic–beam source based on Stern–Gerlach separation [24] and provides an areal target density of about 2×10^{14} (7×10^{13}) atoms/cm^2. The nuclear polarisation of atoms and the atomic fraction are continously measured with a Breit–Rabi polarimeter [25] and a target gas analyser [26], respectively. The polarisation of the atoms can be flipped within short time

intervals providing both helicity states and thus minimising systematic effects in spin–asymmetry measurements.

The average value of the target polarisation for the deuteron (proton) data was 0.85 (0.86) with a fractional systematic uncertainty of 3.5 (4.4)%. The value of the proton target polarisation used for the data presented in this paper has been recalculated making use of improved knowledge of sampling corrections and treatment of molecular polarisation [27]. The luminosity was monitored by detecting Bhabha events using calorimeter detectors close to the beam pipe [28]. The integrated luminosity of the deuteron (proton) data set was 111 pb^{-1} (70 pb^{-1}).

Scattered positrons, as well as coincident hadrons, were detected by the HERMES spectrometer [29]. Positrons were distinguished from hadrons with an average efficiency of 99% and a hadron contamination of less than 1% using the information from an electromagnetic calorimeter, a transition–radiation detector, a preshower scintillation counter and a Cherenkov counter. Only the information on the scattered positron was used in this analysis.

3 Data analysis

In the following, the analysis procedure used for the deuteron data is given. The analysis procedure and systematic uncertainties have been taken from Refs. [19,30] and are detailed in Ref. [20], where the same analysis for the proton was performed. For completeness, the values and parametrisations used in the latter are given below. Note that, compared to Ref. [19], the proton data set has been re–analysed in the full kinematic range in Ref. [20] to optimise the binning of the kinematically more restricted resonance region, where the detector acceptance prevents the full coverage over Q^2.

The kinematic requirements imposed on the scattered positrons in the analysis were identical for both targets. The full range in W^2 ($1.0 < W^2 < 45$ GeV^2) was separated into resonance region ($1.0 < W^2 < 4.2$ GeV^2) and DIS region ($4.2 < W^2 < 45.0$ GeV^2). The Q^2-range $1.2 < Q^2 < 12.0$ GeV^2 was divided into six bins; the same binning as in the proton case was chosen for the analysis of the deuteron data and for the subsequent determination of I^n_{GDH}. After applying data quality criteria, 0.55 (0.13) million events on the deuteron (proton) in the resonance region and 8.3 (1.4) million events in the DIS region were selected.

For all positrons detected, the angular resolution was better than 0.6 mrad, the momentum resolution (aside from Bremsstrahlung tails) better than 1.6% and the Q^2–resolution better than 2.2%. The threshold Cherenkov detector used in the proton measurement was replaced by a Ring–imaging Cherenkov detector [31] for the data taking on the deuteron. The additional amount of material led to a slightly worse W^2–resolution of $\delta W^2 \approx 1.0$ GeV^2 for the deuteron as compared to the proton measurement ($\delta W^2 \approx 0.82$ GeV^2) . Although these W^2–resolutions do not allow distinguishing individual nucleon resonances, the integral measurement in the resonance region is not degraded.

The generalised GDH integral Eq. (2) can be re–written in terms of the longitudinal virtual–photon asymmetry A_1 and the unpolarised structure function F_1:

$$I_{GDH}(Q^2) = \frac{8\pi^2\alpha}{M}\int_0^{x_0}\frac{A_1(x,Q^2)F_1(x,Q^2)}{K}\frac{dx}{x}, \qquad (9)$$

where K is the virtual–photon flux factor chosen in the Gilman convention.

The cross section difference entering the integrand is given by

$$\Delta\sigma = \sigma_{\uparrow\downarrow} - \sigma_{\uparrow\uparrow} = \frac{8\pi^2\alpha}{MK}A_1F_1. \qquad (10)$$

The longitudinal cross–section asymmetry A_1 for the absorption of virtual photons was calculated as

$$A_1 = \frac{A_\parallel}{D} - \eta A_2, \qquad (11)$$

from the measured cross section asymmetry $A_\parallel$, given by

$$A_\parallel = \frac{N^{\uparrow\downarrow}L^{\uparrow\uparrow} - N^{\uparrow\uparrow}L^{\uparrow\downarrow}}{N^{\uparrow\downarrow}L_P^{\uparrow\uparrow} + N^{\uparrow\uparrow}L_P^{\uparrow\downarrow}}. \qquad (12)$$

Here N is the number of detected scattered positrons, L is the integrated luminosity corrected for dead time and L_p is the integrated luminosity corrected for dead time and weighted by the product of the beam and target polarisations. The superscript $\uparrow\uparrow$ ($\uparrow\downarrow$) refers to the orientation of the target spin parallel (anti–parallel) to the positron beam polarisation. The kinematic factor η is given by

$$\eta = \frac{\gamma(1 - y - \gamma^2y^2/4)}{(1 - y/2)(1 + \gamma^2y/2)} \qquad (13)$$

where $y = \nu/E_{beam}$ is the inelasticity of the reaction. The photon depolarisation factor D

$$D = \frac{y(2-y)(1+\gamma^2y/2)}{y^2(1+\gamma^2)(1-2m_e^2/Q^2) + 2(1-y-\gamma^2y^2/4)(1+R)} \qquad (14)$$

depends also on $R = \sigma_L/\sigma_T$, the ratio of the absorption cross sections for longitudinal and transverse virtual photons and the electron mass m_e . A_2 is related to longitudinal–transverse photon–nucleon interference and is not measured in the present experiment. In the DIS region A_2 can be parametrised in a general form as $A_2 = cMx/\sqrt{Q^2}$, where c is a constant determined from world data as $c = 0.05$ (0.53) for the deuteron (proton). In the resonance region no data are available for the deuteron and $A_2 = 0$ was chosen, while for the proton a constant value of $A_2 = 0.06 \pm 0.16$ at $Q^2 = 3$ GeV^2 was adopted [12].

Radiative effects for both targets were calculated using the codes described in Ref. [32]. They were found not to exceed 7% (4%) of the asymmetry A_1 and the deuteron (proton). On the integral level they do not exceed 2% and were included in the systematic uncertainty.

The fraction of events smeared from the DIS to the resonance region and vice versa is evaluated by a Monte

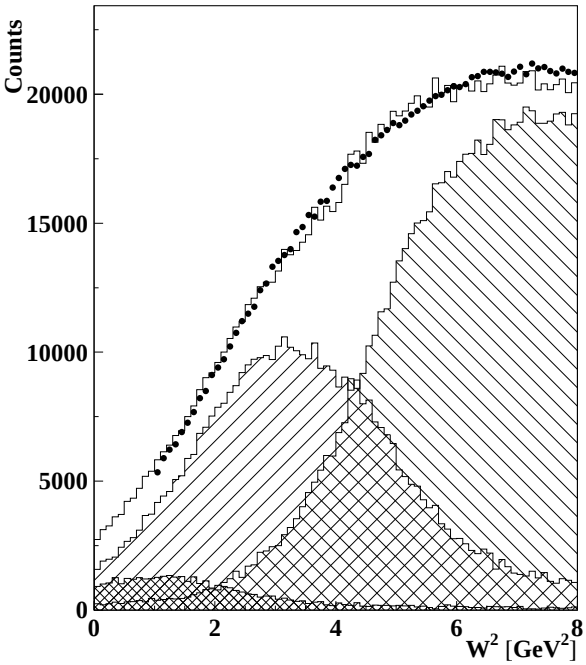

Fig. 1. Data – Monte Carlo comparison for the resonance region as a function of W^2. The cross–hatched area represents the contribution from quasi–elastic scattering, while the lined areas show the contribution from the resonance region (left) itself and from the DIS region (right). The solid line indicates the sum of all simulated events and compares favourably with the data points. The statistical uncertainties of the data are covered by the symbols.

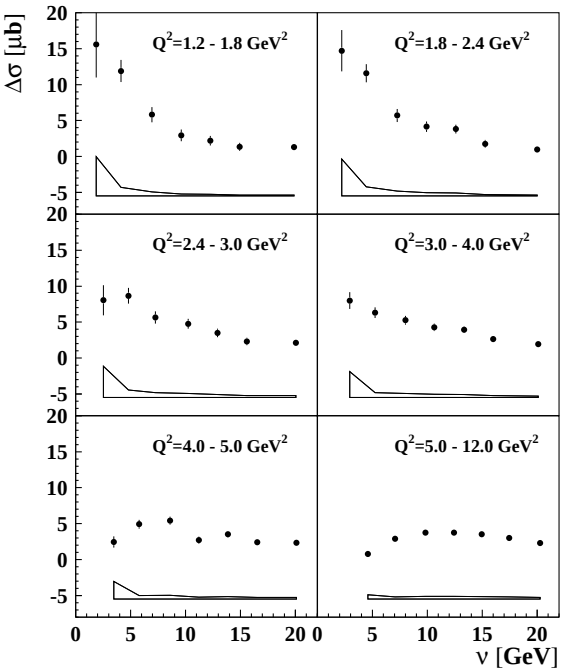

Fig. 2. The cross section difference $\Delta\sigma$ obtained for the Deuteron target as a function of the virtual photon energy ν for different bins in Q^2.

Carlo simulation of both regions including radiative and detector effects. Smearing effects in the deep inelastic region have been evaluated for all targets following the procedures described in Ref. [20]. The events on the deuteron (proton) were simulated using the parametrisation of F_2 from Ref. [33] ([34]) for the DIS region, the elastic form factors from Ref. [35]([36]) and the parameterisation of F_2 in the resonance region from Ref. [37] for both targets. Fig. 1 shows the distribution of experimental data as a function of W^2 in comparison with the simulated events on the deuteron. It is apparent that the shape of the simulated distribution agrees well with the data. Similar agreement has been found for the proton.

For the deuteron (proton) case, the relative contaminations from the elastic and deep inelastic region in the resonance region range from 15% (10%) to 3% (2%) and from 11% (7%) to 23% (16%) respectively, as Q^2 increases from 1.2 GeV^2 to 12.0 GeV^2. The fraction of events smeared from the resonance region to the deep inelastic region ranged from 2.9% (2.5%) to 0.5% (0.2%) respectively. Smearing from the elastic region to the DIS region can be neglected in the present experiment.

To evaluate the systematic uncertainty from smearing, two different assumptions on A_1 for the deuteron (proton) have been used: a polynomial representation $A_1 = -0.0307 + 0.92x - 0.28x^2$ (power law $A_1 = x^{0.727}$) that smoothly extends the DIS behaviour for the asymmetry into the resonance region [38]; and for both targets a step function ($A_1 = -0.5$ for $W^2 < 1.8$ GeV^2 and $A_1 = +1.0$ for 1.8 GeV^2 $< W^2 <$ 4.2 GeV^2) that is suggested by the hypothesis of the possible dominance of the P_{33}–resonance at low W^2 and of the S_{11}–resonance at higher W^2 (see e.g. Ref. [39]). The combined systematic uncertainty from smearing and radiative effects does not exceed 14% (10%) for the deuteron (proton) data. In both cases, smearing gives by far the dominant contribution.

4 Deuteron results

The GDH integrals for the deuteron and proton were evaluated following the procedure described in the previous section. The resonance region and the DIS region were treated separately. The large W^2–range covered by the HERMES experiment allows essentially the first experimental determination of the complete generalised GDH integral for the deuteron, proton and neutron.

The GDH integral I^d_{GDH} for the deuteron was evaluated using Eq. (9) in the resonance region for $1.0 < W^2 < 4.2$ GeV^2 and in the DIS region for $4.2 < W^2 < 45.0$ GeV^2 . The unpolarised structure function $F_1 = F_2(1+\gamma^2)/(2x(1+R))$ was calculated from a modification of the parametrisation of F_2 given in Ref. [37] that accounts for nucleon resonance excitation assuming $R = \sigma_L/\sigma_T$ to be constant and equal to 0.18 in the whole

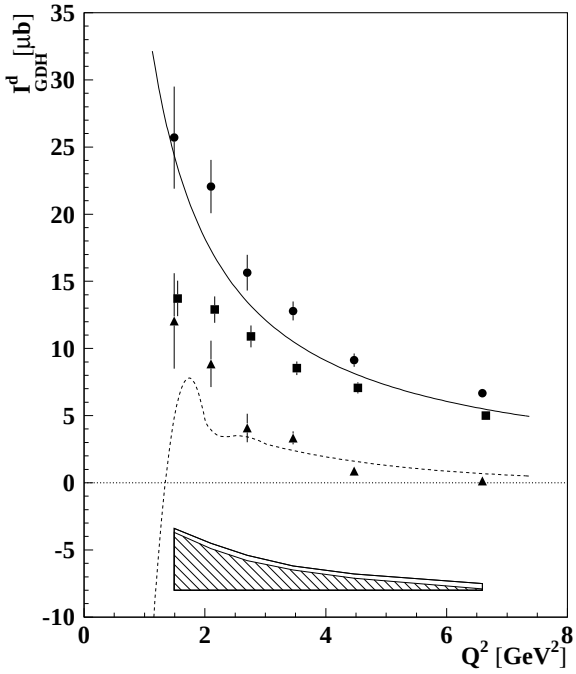

Fig. 3. The generalised GDH integral I^d_{GDH} for the deuteron, shown as a function of Q^2 for the three different kinematic regions considered: resonance region (triangles), DIS region (squares), and full W^2–region including extrapolation to the unmeasured part (circles). The error bars show the statistical uncertainties. The upper curve is taken from Ref. [43], the lower curve represents a model for the resonance region from Ref. [42]. The systematic uncertainties of the full integral are given as a band, the hatched area inside represents the systematic uncertainty of the resonance region alone.

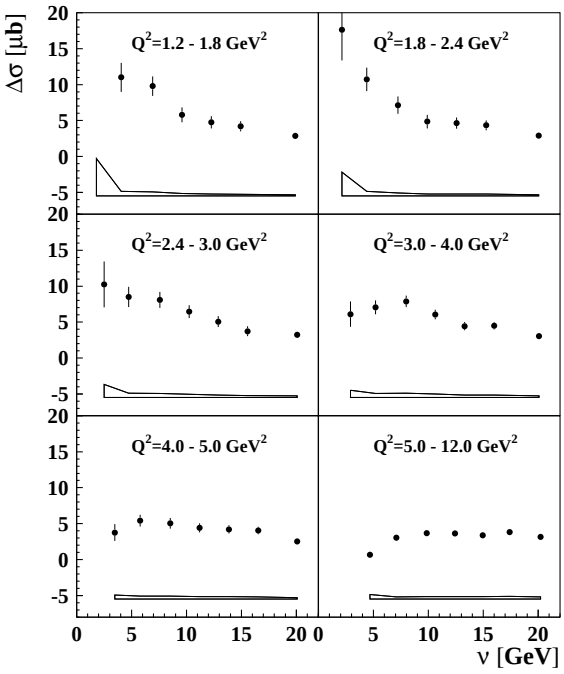

Fig. 4. The cross section difference $\Delta\sigma$ obtained for the proton target as a function of the virtual photon energy ν for different bins in Q^2. Note that for $Q^2 = 1.5$ GeV^2 the first data point corresponding to 28.18 ± 6.79 $\mu b$is off scale.

W^2–range. The unpolarised structure function F_1^d for the deuteron in the DIS region was calculated following a parametrisation of F_2^d from Ref. [33]. In the same kinematic region R was chosen according to a fit in Ref. [40]. Note that due to cancellations between the R dependences of F_1 and D at low y the final result is affected by at most 2% by a particular choice of R. The W^2–dependence of the integrand F_1/K in the individual bins was fully accounted for in the integration.

The extrapolation into the unmeasured region for $W^2 >$ 45 GeV^2 was done using a multiple–Reggeon exchange parametrisation [41] for $\sigma_{\uparrow\downarrow} - \sigma_{\uparrow\uparrow}$ at high energy and ranged from -0.07 μb at $Q^2 = 1.5$ GeV^2 to 1.53 μb at $Q^2 = 6.5$ GeV^2. The corresponding contribution for the proton amounted to about 3.5 μb for all Q^2–bins. The integrand $\Delta\sigma$ used to calculate I^d_{GDH} for the deuteron target is shown in Fig. 2 as a function of ν for the different bins in Q^2. **For the extrapolation into the unmeasured region a fit to the data assuming a c/ν–behaviour with c being a constant was used**

The generalised GDH integrals for the deuteron data, calculated in the resonance region, in the DIS region and over the full W^2–range, are depicted in Fig. 3. The statistical and systematic uncertainties of the full I_{GDH} are clearly dominated by the uncertainties in the resonance region. They are particulary large due to the smallness of D and the large size of η accentuating the uncertainties in A_2, which amounts to 18%. The systematic uncertainty on A_2 in the DIS region does not contribute significantly. The systematic uncertainty for the extrapolation to the unmeasured region at high W^2 of 5% has been taken into account. Further sources of systematic uncertainties include the beam and target polarisations (5.5%), the spectrometer geometry (2.5%), the combined smearing and radiative effects (14%) and the knowledge of F_2 (5%). The total systematic uncertainty with respect to the total GDH integral values amounts to 20% at $Q^2 = 1.5$ GeV^2 to 6% at $Q^2 = 6.5$ GeV^2. For the systematic errors of the resonance and DIS regions independent sources of systematic uncertainty were added in quadrature, while the systematic uncertainty stemming from smearing effects and the knowledge of F_2 were added linearly.

The contribution of the resonance region decreases faster than that of the DIS region as a function of Q^2. The latter dominates I^d_{GDH} for $Q^2 > 3.0$ GeV^2 and remains sizeable even at the lowest measured Q^2. The data in the resonance region shown in Fig. 3, are compared to a curve representing the prediction of the model of Ref. [42]. This model describes the data well for $Q^2 > 2.5$ GeV^2, but underestimates them for lower Q^2. A similar behaviour was observed in Ref. [20] for the proton case shown in Fig. 5. The corresponding values for $\Delta\sigma$ as a function of the virtual photon energy ν in different bins in Q^2 are

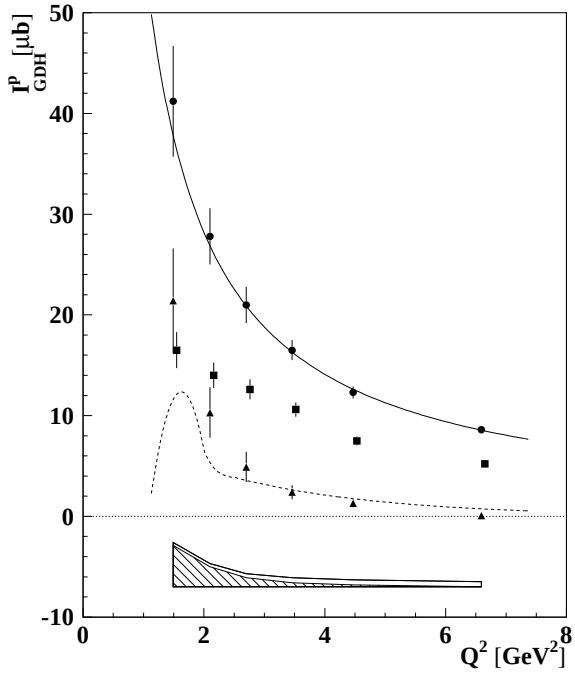

Fig. 5. The generalised GDH integral I^p_{GDH} for the proton using the same notation as in Fig. 3. The upper curve is taken from Ref. [43], the lower curve follows the model of Ref. [42]. The data were published earlier in Ref. [20]. Note that the band representing the systematic uncertainties is given for the convention followed in this paper.

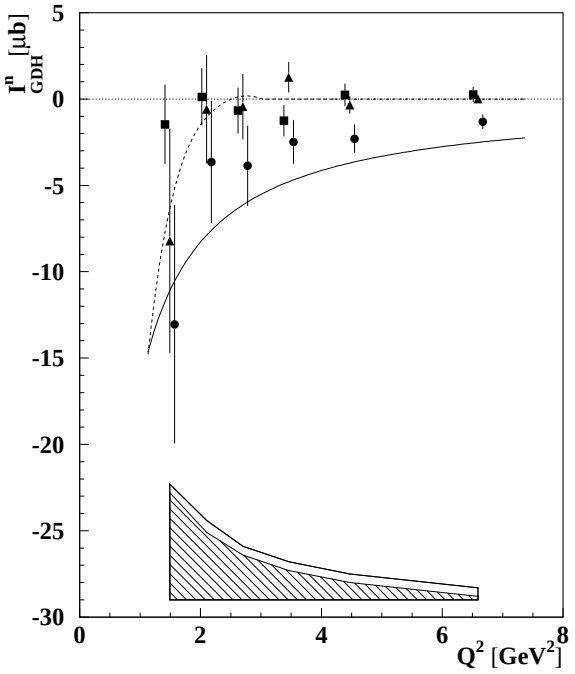

Fig. 6. The generalised GDH integral I^n_{GDH} for the neutron obtained from the deuteron and proton using the same notation as in Fig. 3 for the symbols and theoretical curves.

shown in Fig. 4. Again, the curves represent the Regge behaviour predicted in Ref. [41]. For both targets, the total integral compares favourably with a model based on the Q^2–evolution of the two polarised structure functions g_1 and g_2 without consideration of any explicit nucleon–resonance contribution [43].

5 Neutron results from Deuteron and Proton

Following the formalism described in Ref. [44], the GDH integral I^n_{GDH} for the neutron was calculated from the GDH results on the deuteron I^d_{GDH}, as obtained in this analysis, and those on the proton I^p_{GDH} as presented in Ref. [20]:

$$I^n_{GDH} = \frac{I^d_{GDH}}{1 - 1.5\omega_d} - I^p_{GDH}. \qquad (15)$$

Here $\omega_d = 0.058 \pm 0.010$ [45] is the probability of the deuteron to be in a D–state. It has been shown in Ref. [44] that although the uncertainties in the structure functions being integrated may be large, the resulting uncertainty for the integral does not exceed 3%.

In the real–photon case, the application of Eq. (15) is not straightforward, since significant contributions from photodisintegration and coherent photoproduction must be taken into account [46]. These contributions become negligible at $Q^2 > 1$ GeV^2 and thus will be neglected in the kinematic range under consideration. The application of Eq. (15) and the uncertainty in ω_d lead to an additional systematic uncertainty on I^n_{GDH} of 4%. No further assumptions, in particular not on F^n_2, A^n_2 and R, are needed to derive the generalised GDH integral for the neutron using Eq. (15).

In Fig. 6 the results for I^n_{GDH} obtained from the deuteron data in all kinematic regions are shown together with a model prediction following Ref. [43]. As in the proton case, the contribution from the resonance region decreases faster with increasing Q^2 compared to the contribution from the DIS region. The latter is dominant for $Q^2 > 3.0$ GeV^2 and remains sizeable down to the lowest measured Q^2. In agreement with measurements of the neutron spin structure function g^n_1 and as expected from polarised quark distributions, I^n_{GDH} is negative and of smaller absolute size compared to the proton value.

In contrast to the proton, the model prediction of Ref. [43] does not agree well with the neutron data. This can be attributed to poorer knowledge of the neutron electromagnetic form factors G_E and G_M which are input to this calculation. Furthermore the asymptotic value for Γ^n_1 at high Q^2 is not as precisely known.

Results on I^n_{GDH} were also obtained from a previous measurement on a ^{3}He target [19]. The neutron asymmetry was obtained from the ^{3}He asymmetry taking into account nuclear effects, the relative polarisation of the neutron and two protons, as well as a fit to the data for A^p_1. Note that the lower W^2–limit for the data taken on ^{3}He was 4 GeV^2 and thus slightly different from the cut at 4.2 GeV^2 used in the deuteron analysis. Both data sets are

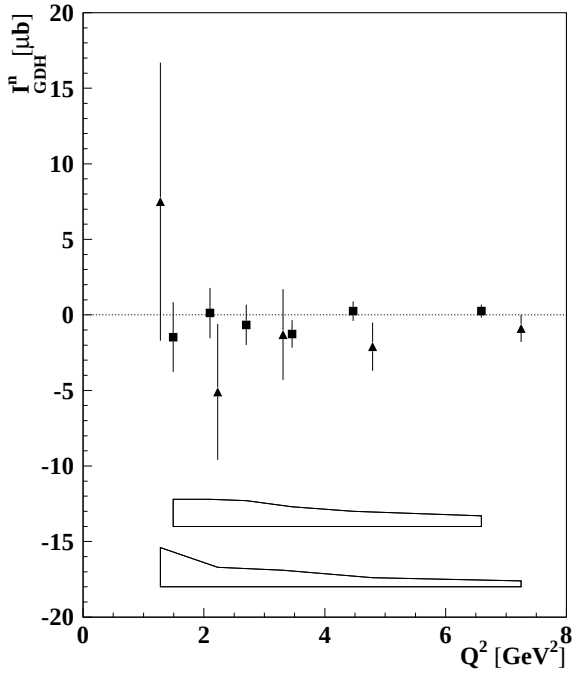

Fig. 7. The generalised GDH integral I^n_{GDH} in the DIS region for the neutron (squares) obtained combining deuteron and proton data, shown in comparison to the results obtained on ^{3}He (triangles) [19]. The lower W^2–limit for the latter was $W^2 > 4.0$ GeV^2 while for the former $W^2 > 4.2$ GeV^2 was used. The error bars represent the statistical uncertainties. The systematic uncertainties for each data set are given as error bands (deuteron top, ^{3}He bottom).

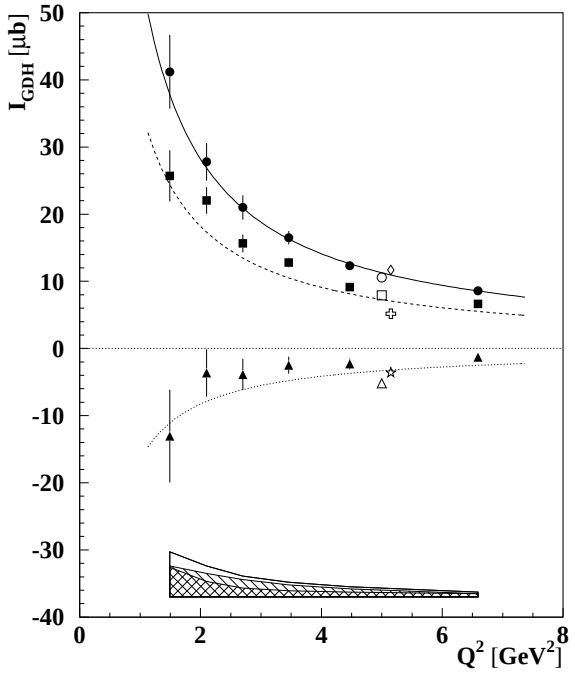

Fig. 8. The Q^2–dependence of the generalised GDH integrals, calculated over the full W^2–region, for the deuteron (squares), proton (circles) and neutron (triangles). The latter was obtained from the deuteron and proton data. The curves shown are the predictions for the different targets according to Ref. [43]. The error bars represent the statistical uncertainties. The bands represent the systematic uncertainties (open: neutron, lined: deuteron, cross–hatched: proton). The open symbols represent the measurements from Ref. [12](left) and Ref. [13](right) on proton, deuteron and neutron, respectively.

shown in Fig. 7 and agree within their respective uncertainties.

6 Discussion of results

In Table 1 the final results are presented for the generalised GDH integrals on the deuteron, the neutron and the proton in the full kinematic range $1.2 < Q^2 < 12.0$ GeV^2 and $1 < W^2 < 45$ GeV^2 and for the three different generalisations (Eqs. 6, 7, 8) considered in the literature. Significant differences between the integral values in different generalisations are observed. While I_A and I_B remain comparable at the measured Q^2 values due to the smallness of γ^2, the $\frac{1}{1-x}$ weighting introduced by the Hand notation in I_C leads to sizeable differences. The results will be discussed referring to the generalisation I_B.

The final results for the proton and for the neutron, as presented in Fig. 5 and Fig. 6, show that the contribution of the resonance region to the full generalised GDH integral is small for $Q^2 > 3$ GeV^2 and the contribution from the DIS region remains sizeable down to the lowest measured Q^2 values. Numerical values following the generalisation I_B are given in Table 2.

All data for the full generalised GDH integrals on the deuteron, proton and neutron are shown together in Fig. 8. They compare favourably to a prediction [43] based on the Q^2–evolution of the two polarised structure functions g_1 and g_2 without consideration of any explicit nucleon–resonance contribution. In the neutron case, the poorer knowledge of input data for this model leads to a larger uncertainty and worse description of the data compared to the proton case. No sign change, as it would be required for the generalised GDH integral on the proton and the deuteron to meet the GDH sum rule prediction at $Q^2 = 0$, is observed in the measured range. Preliminary data from Ref. [17] and a recent theoretical evaluation indicate that this sign change happens at a value of Q^2 lower than the range considered in this analysis [47].

At large Q^2 the generalised GDH integral is connected to the first moment of the spin structure function g_1 (Eq. (4)). For $Q^2 > 3$ GeV^2 the generalised GDH integral is completely dominated by the DIS region. The data presented in this paper agree well with the most recent values for the first moments of the spin structure functions measured on the proton by E–155 (E–143) $\Gamma_1^p = 0.118 \pm 0.004 \pm 0.007$ $(\Gamma_1^p = 0.129 \pm 0.003 \pm 0.010)$ and on the neutron measured by E–154 (E–142) $\Gamma_1^n = -0.058 \pm 0.005 \pm 0.008$ $(\Gamma_1^n = -0.034 \pm 0.007 \pm 0.016)$ evaluated at $Q^2 =$

Table 1. The generalised GDH integral for the deuteron, proton and neutron given in μb for the different generalisation given in Eqs. 6, 7, 8 following Ref. [6] and different values of Q^2 in GeV^2. The statistical and systematic uncertainties are given.

Q^2	1.5	2.1	2.7	3.5	4.5	6.5
I_A^d	29.2 $\pm 4.6 \pm 5.3$	24.6 $\pm 2.4 \pm 3.8$	16.9 $\pm 1.5 \pm 2.8$	13.7 $\pm 0.8 \pm 1.9$	9.5 $\pm 0.5 \pm 1.2$	6.8 $\pm 0.3 \pm 0.5$
I_B^d	25.7 $\pm 3.8 \pm 4.6$	22.1 $\pm 2.0 \pm 3.6$	15.6 $\pm 1.3 \pm 2.6$	12.8 $\pm 0.7 \pm 1.8$	9.1 $\pm 0.5 \pm 1.2$	6.7 $\pm 0.3 \pm 0.5$
I_C^d	47.8 $\pm 9.2 \pm 8.6$	42.8 $\pm 5.1 \pm 6.7$	28.4 $\pm 3.5 \pm 3.9$	24.6 $\pm 1.9 \pm 3.6$	15.2 $\pm 1.3 \pm 2.0$	9.7 $\pm 0.4 \pm 0.8$
I_A^n	-15.1 $\pm 8.4 \pm 7.7$	-3.7 $\pm 4.2 \pm 4.9$	-3.9 $\pm 2.7 \pm 3.4$	-2.3 $\pm 1.4 \pm 2.3$	-2.3 $\pm 0.9 \pm 1.5$	-1.2 $\pm 0.4 \pm 0.7$
I_B^n	-13.1 $\pm 6.9 \pm 6.7$	-3.7 $\pm 3.6 \pm 4.5$	-3.9 $\pm 2.3 \pm 3.1$	-2.5 $\pm 1.3 \pm 2.2$	-2.3 $\pm 0.8 \pm 1.5$	-1.3 $\pm 0.4 \pm 0.7$
I_C^n	-26.6 $\pm 16.8 \pm 12.6$	-4.7 $\pm 9.2 \pm 8.5$	-3.9 $\pm 6.4 \pm 4.8$	0.1 $\pm 3.4 \pm 4.2$	-3.1 $\pm 2.3 \pm 2.5$	-0.8 $\pm 0.6 \pm 1.1$
I_A^p	47.0 $\pm 6.7 \pm 5.0$	30.6 $\pm 3.3 \pm 2.5$	22.4 $\pm 2.1 \pm 1.4$	17.3 $\pm 1.1 \pm 1.0$	12.8 $\pm 0.7 \pm 0.7$	8.7 $\pm 0.3 \pm 0.5$
I_B^p	41.2 $\pm 5.5 \pm 5.4$	27.8 $\pm 2.8 \pm 2.3$	21.0 $\pm 1.8 \pm 1.3$	16.5 $\pm 1.0 \pm 0.9$	12.3 $\pm 0.6 \pm 0.7$	8.6 $\pm 0.3 \pm 0.5$
I_C^p	78.9 $\pm 13.5 \pm 8.4$	51.6 $\pm 7.4 \pm 4.4$	36.1 $\pm 5.1 \pm 2.2$	26.9 $\pm 2.7 \pm 1.5$	19.7 $\pm 1.8 \pm 1.1$	11.4 $\pm 0.4 \pm 0.7$

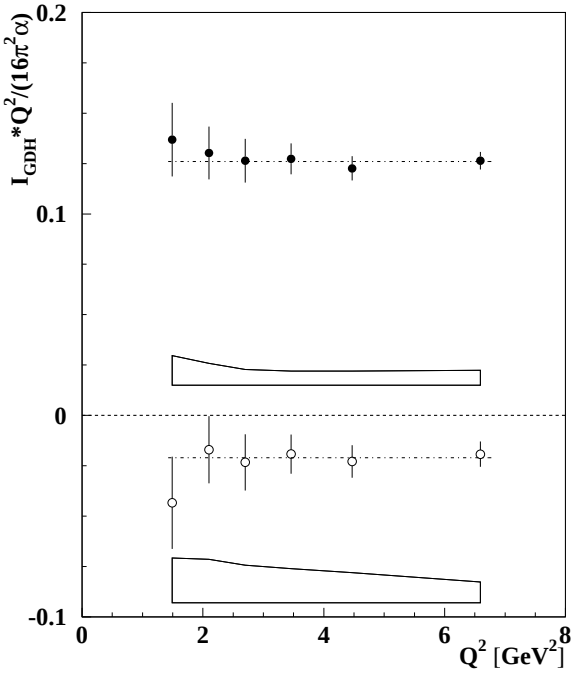

Fig. 9. The Q^2–dependence of the generalised GDH integrals for the proton (filled circles) and neutron(open circles) after the leading–twist dependence, $Q^2/(16\pi^2\alpha)$, has been divided out. The error bars represent the statistical errors. The systematic uncertainties are represented by the respective error bands. The dash–dotted lines are straight line fits to the data.

5 GeV^2 [12,13]. These values correspond to $I^p_{GDH}(Q^2 = 5\ \mathrm{GeV}^2) = 10.59 \pm 0.36 \pm 0.73$ $(11.85 \pm 0.28 \pm 0.92)$ μb and $I^n_{GDH}(Q^2 = 5\ \mathrm{GeV}^2) = -5.21 \pm 0.45 \pm 0.72$ $(-3.12 \pm 0.64 \pm 1.47)$ μb respectively and are shown together with the present data in Fig. 8. The difference in the first moments extracted from E–143 and E–155 can be mainly attributed to the different scheme used to extrapolate into the unmeasured region. The extrapolation method used by E–143 corresponds to the method adopted in this paper.

The Q^2–behaviour of I_{GDH} for proton and neutron can be more clearly studied when dividing out from I_{GDH} the Q^2–dependence expected from leading twist, $16\pi^2\alpha/Q^2$, as shown in Fig. 9. Any contributions from resonance form factors or higher–twist contributions should become visible as a deviation from a flat line. Within the statistical and systematic uncertainties of the present measurement no deviation from a leading–twist behaviour can be seen. In other words, the experimental data obtained for the proton and the neutron are consistent with the naive expectation that the $1/Q^2$ expansion is a good approximation down to $Q^2 \simeq 2$ GeV^2. As discussed in the introduction the elastic part ($x = 1$) has to be included for a complete comparison to a twist expansion of Γ_1 . However, this is not a relevant contribution in the kinematic range considered.

7 Combined results for the Proton and the Neutron

The data obtained for the proton and neutron over a large range in Q^2 and W^2 offer a unique possibility to evaluate the proton–neutron difference of the generalised GDH integral. This difference is shown in Fig. 10. In accordance to the GDH sum rule prediction for $Q^2 = 0$ no sign change at low Q^2 is observed. The data fall off as $1/Q^2$ indicating that leading twist dominates. A fit to the data using c/Q^2 where c is a constant is shown together with the data in Fig. 10. For the constant $c = 66 \pm 2$ is found, leading to a value $I^{p-n}_{GDH}(Q^2 = 5\ \mathrm{GeV}^2) = 13.2 \pm 0.8 \pm 1.2\ \mu b$. At $Q^2 = 5$ GeV^2 they are in agreement with an experimental determination of the Bjorken sum rule by E–155 (E–143), $\Gamma_1^p - \Gamma_1^n = 0.176 \pm 0.003 \pm 0.007$ $(0.164 \pm 0.008 \pm 0.020)$ [12,13] within the respective experimental uncertainties. At $Q^2 = 5$ GeV^2 these values correspond to $I^{p-n}_{GDH} = 15.76 \pm 0.27 \pm 0.63\ \mu b$ $(14.95 \pm 0.74 \pm 1.84\ \mu b)$. Within errors, the value for the proton–neutron difference measured in this analysis is also in agreement with the Bjorken–sum–rule prediction of 0.182 ± 0.005 corresponding $I^{p-n}_{GDH} = 16.33 \pm 0.45\ \mu b$. The Bjorken sum rule was evaluated following Eq. (5) at $Q^2 = 5$ GeV^2

Table 2. The generalised GDH integral I_B for the deuteron, proton and neutron given in μb for the full region, the resonance region and the DIS region and different values of Q^2 in GeV^2. The last two rows show the integral values for the extrapolation to higher W^2, for the proton and the deuteron.

Q^2	1.5	2.1	2.7	3.5	4.5	6.5
$I^d_{\rm tot}$	25.7±3.8 ± 4.6	22.1±2.0 ± 3.6	15.6±1.3 ± 2.6	12.8±0.7 ± 1.8	9.1±0.5 ± 1.2	6.7±0.3 ± 0.5
$I^d_{\rm res}$	12.1±3.6 ± 4.3	8.9±1.8 ± 3.1	4.1±1.1 ± 2.2	3.3±0.5 ± 1.5	0.9±0.3 ± 0.9	0.1±0.1 ± 0.1
$I^d_{\rm DIS}$	13.7±1.3 ± 1.4	12.9±1.0 ± 1.4	10.9±0.8 ± 1.3	8.5±0.5 ± 0.9	7.0±0.4 ± 0.7	5.0±0.3 ± 0.5
$I^p_{\rm tot}$	41.2±5.5 ± 4.4	27.8±2.8 ± 2.3	21.0±1.8 ± 1.3	16.5±1.0 ± 0.9	12.3±0.6 ± 0.7	8.6±0.3 ± 0.5
$I^p_{\rm res}$	21.4±5.2 ± 4.1	10.3±2.5 ± 2.0	4.9±1.5 ± 0.9	2.4±0.7 ± 0.4	1.3±0.4 ± 0.2	0.1±0.1 ± 0.1
$I^p_{\rm DIS}$	16.5±1.8 ± 1.0	14.0±1.3 ± 0.9	12.6±1.0 ± 0.9	10.6±0.7 ± 0.8	7.5±0.5 ± 0.6	5.2±0.3 ± 0.5
$I^n_{\rm tot}$	−13.1±6.9 ± 6.7	−3.7±3.6 ± 4.6	−3.9±2.3 ± 3.1	−2.5±1.3 ± 2.2	−2.3±0.8 ± 1.5	−1.3±0.4 ± 0.7
$I^n_{\rm res}$	−8.2±6.5 ± 6.2	−0.6±3.2 ± 3.9	−0.4±1.9 ± 2.6	1.3±0.9 ± 1.7	−0.3±0.5 ± 1.0	0.1±0.1 ± 0.2
$I^n_{\rm DIS}$	−1.5±2.3 ± 1.8	0.1±1.7 ± 1.8	−0.7±1.3 ± 1.7	−1.3±0.9 ± 1.3	0.2±0.7 ± 1.0	0.3±0.4 ± 0.7
$I^d_{\rm unm}$	−0.07	0.3	0.65	0.92	1.18	1.53
$I^p_{\rm unm}$	3.3	3.5	3.5	3.5	3.5	3.3
$I^n_{\rm unm}$	−3.4	−3.2	−2.8	−2.5	−2.2	−1.6

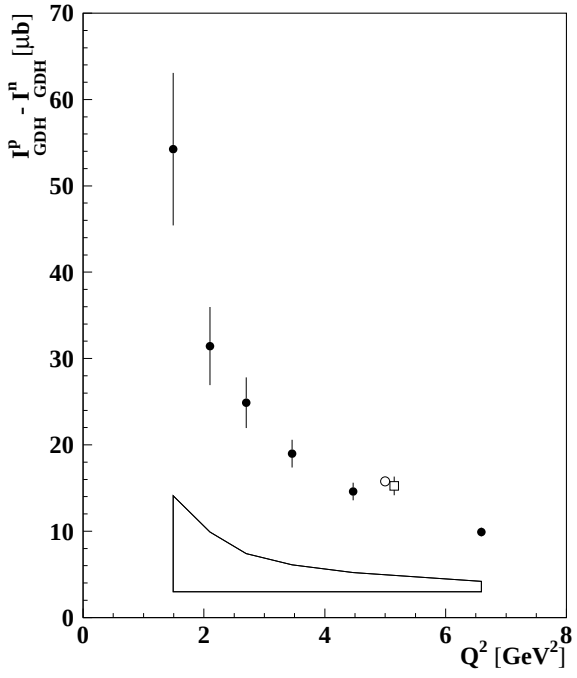

Fig. 10. The Q^2–dependence of the generalised GDH integral for the proton–neutron difference. The curve represents a simple $1/Q^2$ fit to the data leading to $I^{p-n}_{GDH}(Q^2 = 5\ \text{GeV}^2)$ of 13.2 ±0.8 ± 1.2 μb. For large Q^2 this difference is expected to obey the Bjorken sum rule. The open symbols represent the measurements of the Bjorken sum rule from Refs. [12] (square) and [13] (circle). They are slightly shifted in Q^2 for clearer representation. At $Q^2 = 0$ the GDH sum rule gives a value of 29 μb. The error bars represent the combined statistical uncertainties, the band indicates the systematic uncertainty.

including corrections up to third–order in α_s and using $\alpha_s(M_Z) = 0.118$.

8 Summary

The generalised GDH integral has been determined for a deuteron target in the kinematic region $1.2 < Q^2 < 12.0$ GeV^2 and $1 < W^2 < 45$ GeV^2 in this paper, while a corresponding re–analysis of the HERMES proton data was already described in Ref. [20]. In both cases the W^2–range was separated at $W^2 = 4.2$ GeV^2 into a region where the nucleon resonances dominate and into the DIS region. Combining both data sets the generalised GDH integral for the neutron was calculated in the same kinematic regions. These neutron results obtained from the deuteron agree with those obtained earlier on a ^{3}He target in the same kinematic region.

Altogether, a complete measurement of the generalised GDH integrals for the deuteron, proton and neutron is available. In all three cases the resonance contribution to the generalised integral decreases rapidly with increasing Q^2 and the contribution from the DIS region is still sizeable even at the lowest measured Q^2 emphasizing the importance of measuring the GDH integral over a large W^2–range. At larger Q^2 the measured values agree with data on the first moment of the spin structure function g_1.

For the generalised GDH integrals of the proton, the neutron and the proton–neutron difference the Q^2–dependence is in agreement with a leading–twist behaviour; within the experimental uncertainties it exhibits no significant contribution from either higher twist or resonance form factors. The proton–neutron difference is in agreement with the Bjorken–sum–rule prediction evaluated at $Q^2 = 5$ GeV^2 within the experimental uncertainties.

We gratefully acknowledge the DESY management for its support, the staffs at DESY and the collaborating institutions for

their significant effort. This work was supported by the FWO–Flanders, Belgium; the Natural Sciences and Engenieering Research Council of Canada; the INTAS and TMR network contributions from the European Community; the German Bundesministerium für Bildung und Forschung; the Deutsche Forschungsgemeinschaft (DFG); the Deutscher Akademischer Austauschdienst (DAAD); the Italian Istituto Nazionale di Fisica Nucleare (INFN); Monbusho International Scientific Research Program, JSPS, and Toray Science Foundation of Japan; the Dutch Foundation for Fundamenteel Onderzoek der Materie (FOM); the U. K. Particle Physics and Astronomy Research Council; and the U. S. Department of Energy and National Science Foundation.

References

1. S.B. Gerasimov, Sov. J. Nucl. Phys. **2** (1966) 430; S.D. Drell and A.C. Hearn, Phys. Rev. Lett. **16** (1966) 908.
2. J. Ahrens *et al.*, Phys. Rev. Lett. **87** (2001) 022003.
3. G. Zeitler, Proceedings of *MENU 2001*, Washington D. C., 2001, to be published in πN–Newsletter.
4. V. Ghazikhanian *et al.*, SLAC–Proposal E–159 (2000); D.Sober *et al.*, CEBAF PR–91–15 (1991).
5. R. Pantförder, PhD Thesis, Universität Bonn (1998), BONN-IR-98-06, hep-ph/9805434 and reference therein.
6. D. Drechsel, S.S. Kamalov and L. Tiator, Phys. Rev. **D 63** (2001), 114010.
7. X. Ji and W. Melnitchouk, Phys. Rev. **D 56** (1997) R1.
8. I. Karliner, Phys. Rev. **D 7** (1973) 2717; R.L. Workman and R.A. Arndt, Phys. Rev. **D 45** (1992) 1789; A.M. Sandorfi, C.S. Whisnant and M. Khandaker, Phys. Rev. **D 50** (1994) R6681; D. Drechsel and G. Krein, Phys. Rev. **D 58** (1998) 116009.
9. J.D. Bjorken, Phys. Rev. **148** (1966) 1467; Phys. Rev. **D 1** (1970) 1376.
10. Particle Data Group, Eur. Phys. J. **C 15** (2000) 1.
11. S. A. Larin, J. A. M. Vermaeseren, Phys. Lett. **B 259** (1991) and references therein.
12. E143 Collaboration, K. Abe *et al.*, Phys. Rev. **D 58** (1998) 112003.
13. E155 Collaboration, P. L. Anthony *et al.*, Phys. Lett. **B 493** (2000) 19; E155 Collaboration, P. L. Anthony *et al.*, Phys. Lett. **B 463** (1999) 339.
14. SMC Collaboration, B. Adeva *et al.*, Phys. Rev. **D 58** (1998) 112002.
15. F.J. Gilman, Phys. Rev. **167** (1968) 1365.
16. L. N. Hand, Phys. Rev. **129** (1963) 1834.
17. V. Burkert *et al.*, CEBAF PR-91-23, 1991; S. Kuhn *et al.*, CEBAF PR-93-09, 1993; Z.E. Meziani *et al.*, CEBAF PF-94-10, 1994; J.P. Chen *et al.*, TJANF PR-97-110, 1997.
18. M. Amarian *et al.*, `nucl--ex/0205020`
19. HERMES Collaboration, K. Ackerstaff *et al.*, Phys. Lett. **B 444** (1998) 531.
20. HERMES Collaboration, A. Airapetian *et al.*, Phys. Lett. **B 494** (2000) 1.
21. D.P. Barber *et al.*, Phys. Lett. **B 343** (1997) 436.
22. M. Beckmann *et al.*, Nucl. Instr. Meth. **A 479** (2002) 334.
23. J. Stewart, Proc. of the Workshop on Polarised gas targets and polarised beams, edited by R.J. Holt and M.A. Miller, Urbana-Champaign, USA, AIP Conf. Proc. **421** (1997) 69.
24. F. Stock *et al.*, Nucl. Instr. and Meth. **A 343** (1994) 334.
25. C. Baumgarten *et al.*, Nucl. Instr. and Meth. **A** , in press.
26. M. C. Simani *et al.*, submitted to Nucl. Instr. and Meth. **A**.
27. HERMES Collboration, target paper in preparation
28. Th. Benisch *et al.*, Nucl. Instr. and Meth. **A 471** (2001) 314.
29. HERMES Collaboration, K. Ackerstaff *et al.*, Nucl. Instr. and Meth. **A 417** (1998) 230.
30. HERMES Collaboration, A. Airapetian *et al.*, Phys. Lett. **B 442** (1998) 484.
31. N. Akopov et al., Nucl. Instr. and Meth. **A 479** (2002) 511.
32. I.V. Akushevich and N.M. Shumeiko, J. Phys. **G 20** (1994) 513; I. Akushevich *et al.*, Comput. Phys. Commun. **104** (1997) 201.
33. NMC Collaboration, M. Arneodo *et al.*, Nucl. Phys. **B 371** (1992) 3.
34. NMC Collaboration, M. Arneodo *et al.*, Phys. Lett. **B 36 4** (1995) 107.
35. S. Stein *et al.*, Phys. Rev. **D 12** (1975) 1884 and references therein.
36. S. I. Bilen'kaya *et al.*, Zh. Eksp. Teor. Fiz. Pis'ma **19** (1974) 613.
37. A. Bodek, Phys. Rev. **D 8** (1973) 2331.
38. A. P. Nagaitsev *et al.*, JINR Rapid Communications, July 1995, N3(71)-95,59.
39. J. Edelmann, G. Piller, N. Kaiser and W. Weise, Nucl. Phys. **A 665** (2000) 125.
40. L.W. Whitlow *et al.*, Phys. Lett. **B 250** (1990) 193.
41. N. Bianchi and E. Thomas, Phys. Lett. **B 450** (1999) 439.
42. I. G. Aznauryan, Phys. of At. Nucl. **58** (1995) 1014 and private communication.
43. J. Soffer and O.V. Teryaev, Phys. Rev. **D 51** (1995) 25; J. Soffer and O.V. Teryaev, Phys. Rev. Lett. **70** (1993) 3373.
44. C. Ciofi degli Atti *et al.*, Phys. Lett. **B 376** (1996) 309.
45. M. Lacombe *et al.*, Phys. Lett. **B 101**(1981) 139.
46. H. Arenhövel, G. Kreß, R. Schmidt, P. Wilhelm, Phys. Lett. **B 407** (1997) 1.
47. X. Ji, C.W. Kao and J. Osborne, Phys.Rev. **D 61** (2000) 074003 ; X. Ji and J. Osborne, J. Phys. **G 27** (2001) 127.